NANO · MICRO
small

Supporting Information

for *Small*, DOI 10.1002/smll.202408217

Reversible Sliding Motion by Hole-Injection in Ammonium-Linked Ferrocene, Electronically Decoupled from Noble Metal Substrate by Crown-Ether Template Layer

Fumi Nishino, Peter Krüger, Chi-Hsien Wang, Ryohei Nemoto, Yu-Hsin Chang, Takuya Hosokai, Yuri Hasegawa, Keisuke Fukutani, Satoshi Kera, Masaki Horie and Toyo Kazu Yamada**

Supplementary Information

Reversible Sliding Motion by Hole-Injection in Ammonium-Linked Ferrocene, Electronically Decoupled from Noble Metal Substrate by Crown-Ether Template Layer

Fumi Nishino[1], Peter Krüger[1,2], Chi-Hsien Wang[3], Ryohei Nemoto[1], Yu-Hsin Chang[3], Takuya Hosokai[4], Yuri Hasegawa[5], Keisuke Fukutani[5], Satoshi Kera[5], Masaki Horie[3*] and Toyo Kazu Yamada[1,2*+]

1. Department of Materials Science, Chiba University, 1-33 Yayoi-Cho, Inage-Ku, Chiba 263-8522, Japan.

2. Molecular Chirality Research Centre, Chiba University, 1-33 Yayoi-cho, Inage-Ku, Chiba 263-8522, Japan.

3. Department of Chemical Engineering, National Tsing Hua University, 101, Sec. 2, Kuang-Fu Road, Hsinchu, 30013, Taiwan

4. National Institute of Advanced Industrial Science and Technology, National Metrology Institute of Japan, Tsukuba Central 5, 1-1-1, Higashi, Tsukuba, Ibaraki 305-8565, Japan

5. Institute for Molecular Science, Myodaiji, Okazaki 444-8585 Japan

Author Information,

Corresponding Author: Toyo Kazu Yamada *E-mail: **toyoyamada@faculty.chiba-u.jp**

Corresponding Author: Masaki Horie *E-mail: **mhorie@mx.nthu.edu.tw**

Version 2024.11.28

Movie S1: **Bias-dependent structure variations.** STM topographic images of Fc-amm 2D array on the BrCR nanoporous SAM film.

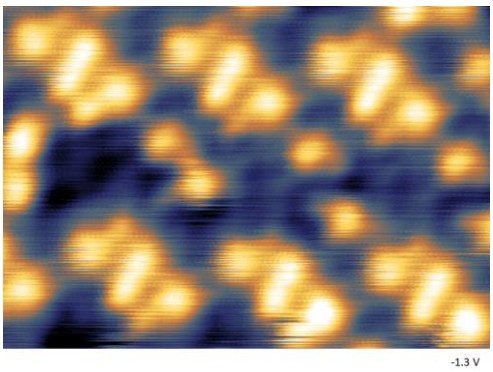

Movie S2: **Current-dependent structure variations.** STM topographic images of Fc-amm 2D array on the BrCR nanoporous SAM film.

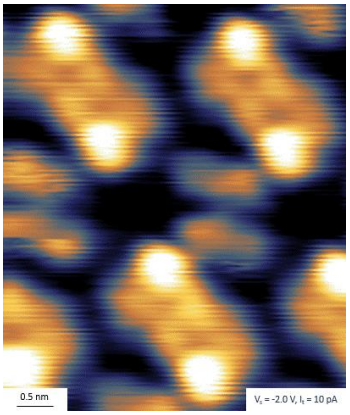

Movie S3: **Bias-dependent LDOS variations.** STS d*I*/d*V* maps of Fc-amm 2D array on the BrCR nanoporous SAM film.

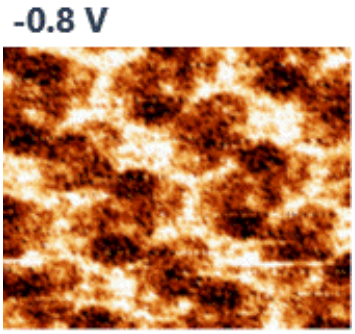

Figure S1 FDMS of sublimates using [ferrocenylmethyl(methyl)ammonium]$^{+}(PF_6)^{-}$.

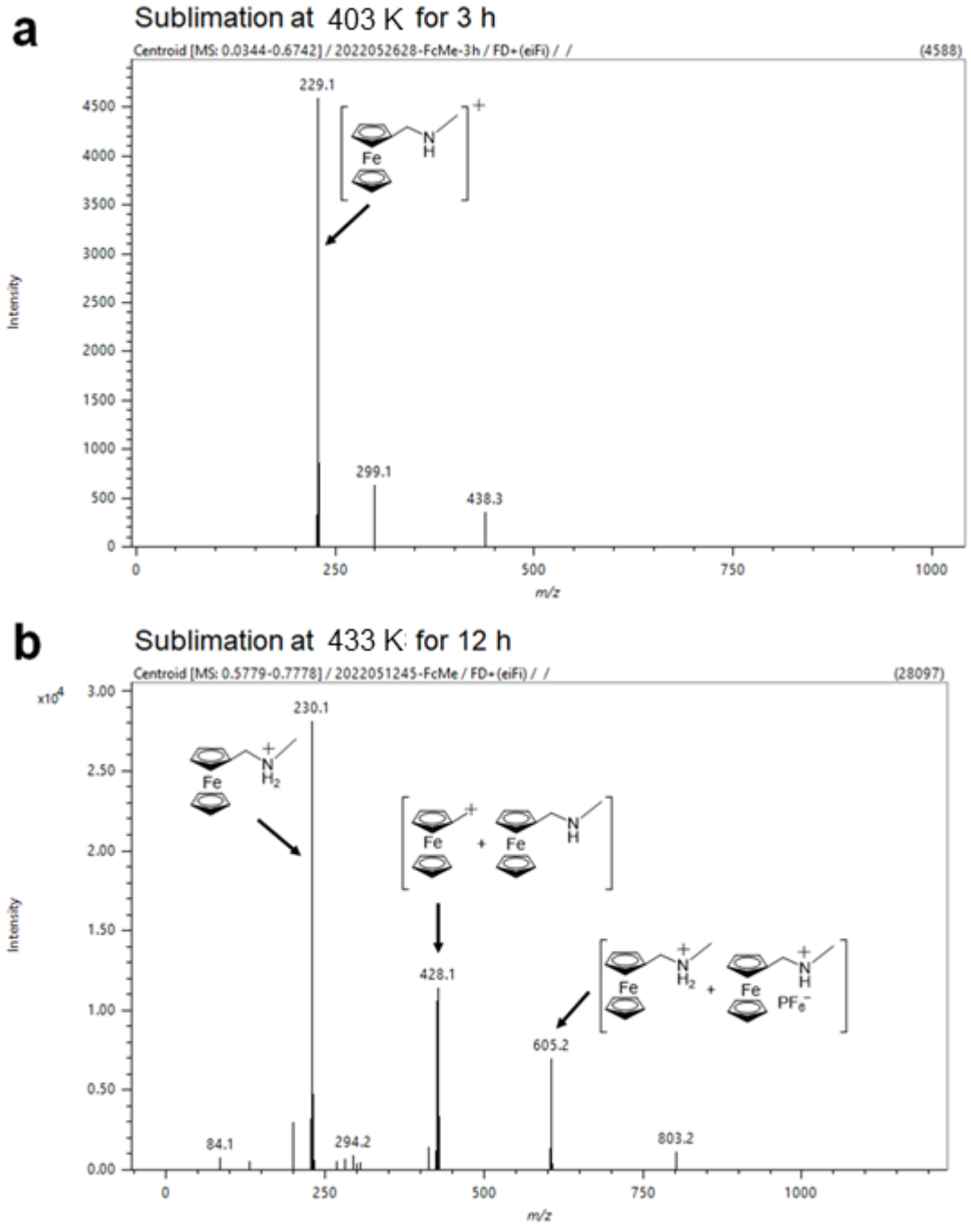

Figure S1. FDMS of sublimates using [ferrocenylmethyl(methyl)ammonium]$^{+}(PF_6)^{-}$. (a) Sublimation at 403 K for 3 h. The main peak at m/z = 229.1 corresponds to $[C_{12}H_{15}FeN]^{+}$ = 229.1. (b) Sublimation at 433 K for 12 h. The main peak at m/z = 230.1 corresponds to $[C_{12}H_{16}FeN]^{+}$ = 230.1. Plausible chemical structures are shown in the figures.

Table S1 Crystal data and details structure refinement**.**

	A1
Temp./K	100
Formula	$C_{64}H_{71}Br_8F_{12}Fe_2N_2O_{12}P_2$
molecular weight	2101.14
crystal system	Monoclinic
space group	*C 1 2/c 1*
a/ Å	44.9404(10)
b/ Å	11.6385(3)
c/ Å	29.9293(6)
α/deg	90
β/deg	106.875(2)
γ/deg	90
V/ Å^3	14980.1(6)
Z	8
μ(CuKα)/Å	1.54184
F(000)	8280
D/g cm^{-3}	1.863
crystal size/mm^3	0.23 x 0.03 x 0.01
reflections collected	13274
used reflections	12995
R	0.0672
*R*w	0.1727
GOF	1.033

Figure S2, Cleaning condition of Cu(111) surface.

We used the Cu(111) single crystal as a substrate because the previous research reported the successful growth of a well-ordered BrCR molecular on Cu(111) at 300 K in ultra-high vacuum (UHV). Furthermore, it is noteworthy that the BrCR ring undergoes flattening upon its adsorption onto the

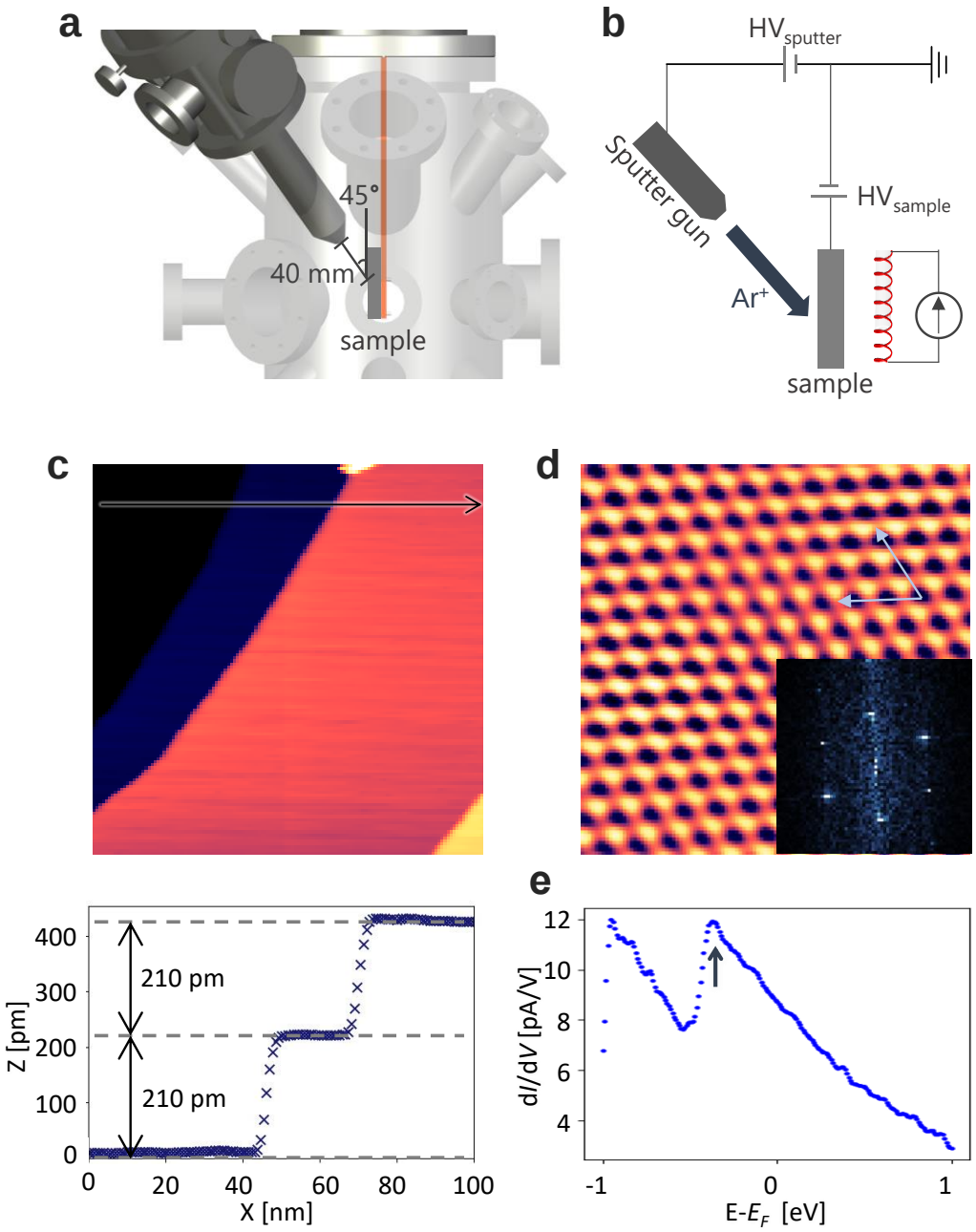

Figure S2. (a) Cleaning setup of the sputter gun and the sample stage. (b) Electronic circuit diagram during the sputter and the sample heating. We used electron bombardment heating. (c-e) STM / STS study on the cleaned Cu(111). (c) STM image obtained on the cleaned Cu(111) atomic terraces (200 nm × 200 nm, V_s = 1.0 V, I_t = 100 pA). The height profile along the arrow shows the step height of ~210 pm in agreement with the bulk fcc-Cu(111) layer distance of 208 pm. (d) Atomically resolved STM image obtained on Cu(111) terrace (3 nm × 3 nm, V_s = 1.0 V, I_t = 100 pA). The inset denotes the fast Fourier-transformed (FFT) image. (e) STS dI/dV curve obtained on the Cu(111) surface. E_F denote the Fermi energy.

Cu(111) substrate. The Cu(111) substrate was carefully sputtered and annealed to obtain clean, atomically flat surfaces (Figs. S1a and S1b). Figure S1c shows an STM topographic image obtained on the Cu(111) surface, revealing the monolayer step with a height of approximately 210 pm. The STM atomically-resolved image and the fast Fourier transformed (FFT) image in Fig. S1d manifest six-fold distinct spots corresponding to the fcc(111) symmetry. Scanning tunneling spectroscopy (STS) showed the Cu(111) surface state peak at −0.35 eV, as illustrated in Fig. S1e.

Figure S3, Molecular evaporator

A custom-fabricated molecular evaporator (Fig. S3b) was installed within the introduction chamber of our UHV-STM setup (Fig. S3). The spatial separation between the apex of the evaporator and the specimen is approximately 55 mm, with an incident angle of roughly 20 degrees relative to the vertical direction. The quantity of sublimated molecules was meticulously regulated through the utilization of the quartz crystal microbalance (QCM).

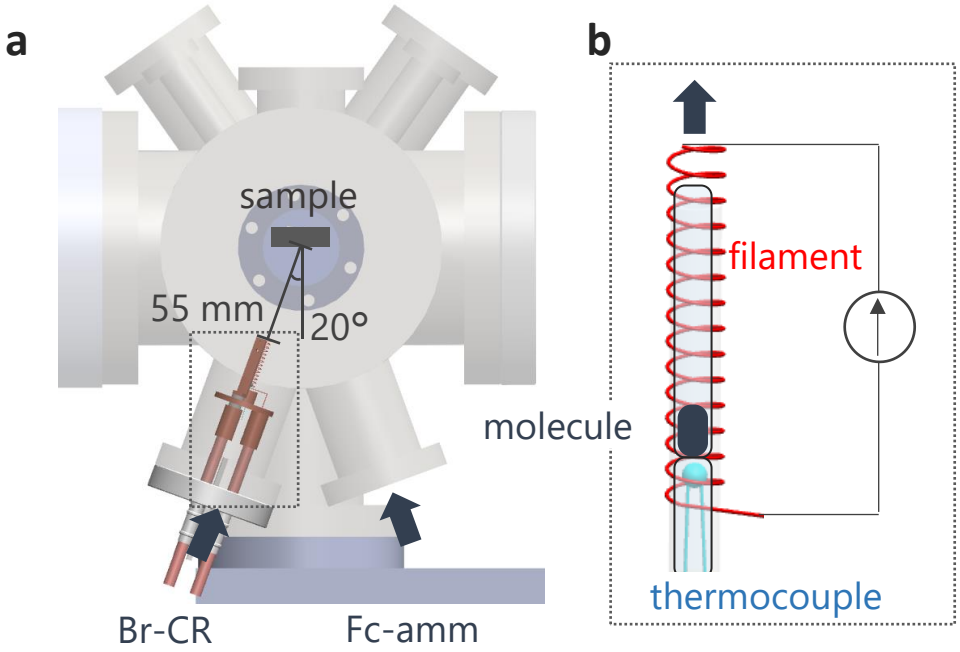

Figure S3. Home-built STM molecular evaporator set into the introduction chamber of our UHV-STM setup. BrCR and Fc-amm powders (~10 mg) were set inside the quartz crucible (~50 mm length). The thermocouple monitored the crucible temperature.

Figure S4, BrCR array on Cu(111)

The CR cyclic ring molecules have been employed for capturing guest metal atoms, ions, or molecules within the ring. In this study, BrCR was utilized, giving rise to the 2D SAM array on the atomically flat and pristine Cu(111) surface. Figure S4a depicts the STM topographic image obtained on the Cu(111) surface after depositing approximately 0.5 MLs of BrCR. The BrCR array manifests a height of approximately 240 pm, as illustrated in the lower panel of Fig. S4a. The magnified image in Fig. S4b delineates the alignment of BrCR, illustrating the unit cell using arrows and lines. The d*I*/d*V* curve in Fig. S4c illustrates the HOMO peak at -1.5 eV and the LUMO peak detected at +1.3 eV.

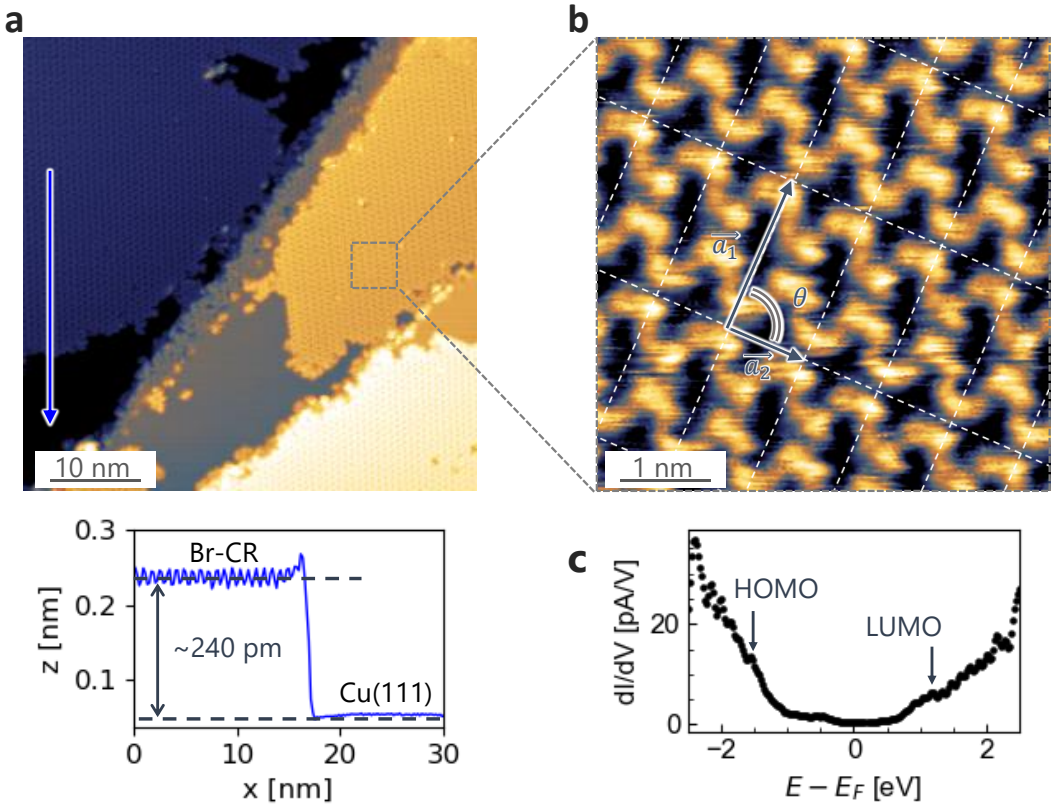

Figure S4. (a) STM topographic image obtained on the Cu(111) surface after depositing 0.5 MLs of BrCR (50 nm × 50 nm, V_s = 1.5 V, I_t = 10 pA). The lower panel denotes the height profile along the arrow. (b) Enlarged STM topographic image obtained within the BrCR island (5 nm × 5 nm, V_s = 750 mV, I_t = 10 pA). (c) d*I*/d*V* curve obtained on the BrCR island.

Figure S5, Fc-amm molecules on Cu(111).

The STM examination was executed on the Cu(111) surface after depositing 0.2 MLs of the Fc-amm at 300 K in a UHV environment. The STM topographic representation in Fig. S5a delineates the thermally diffused Fc-amm molecules, forming monolayer height islands along the Cu steps. The height profiles along the indicated arrows in Fig. S5a elucidate the Fc-amm islands' elevation, measuring approximately 330 pm, surpassing the Cu step height of approximately 210 pm (as illustrated in Fig. S5c). The magnified STM image in Fig. S5b, focusing within the Fc-amm island, reveals numerous protrusions categorized into two types: brighter and darker spots, indicative of a

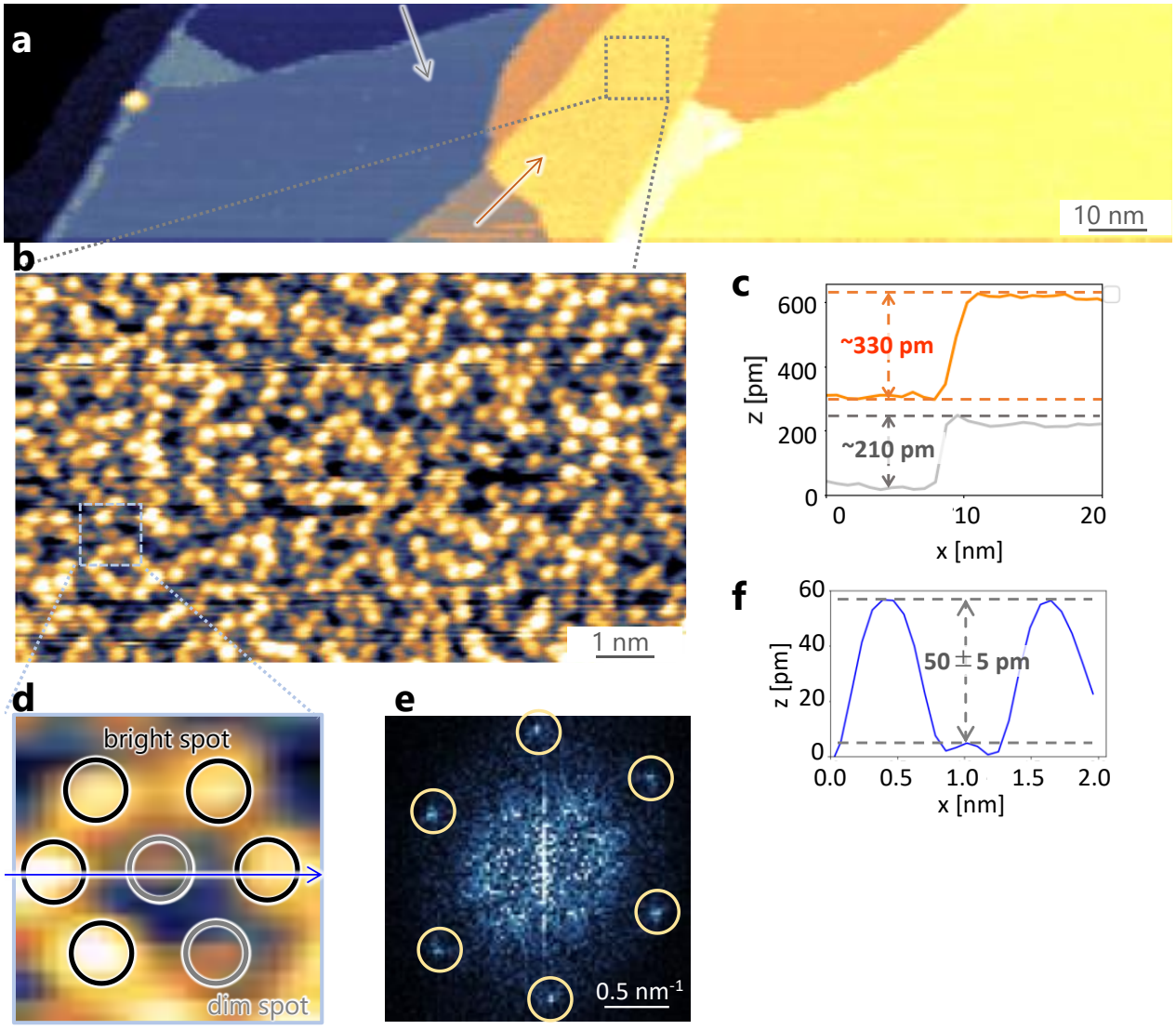

Figure S5. STM results obtained on the Cu(111) surface covered by the 0.2 MLs Fc-amm at 300 K in UHV. (a) STM topographic image: 200 nm × 40 nm, V_s = 2.5 V, I_t = 15 pA. (b) Enlarged STM image inside the Fc-amm island: 20 nm × 10 nm, V_s = 1.5 V, I_t = 60 pA. (c) Height profiles along the orange and grey arrows in (a). (d) Further enlarged STM image of the Fc-amm protrusions. (e) The FFT image obtained from (b). (f) The height profile along the arrow in (d).

height disparity of around 50 pm (refer to the magnified images in Figs. S5d and S5f). The brighter and darker spots can be ascribed to face-on and edge-on Fc adsorptions. Considering the fast Fourier transformed (FFT) image derived from Fig. S5b, which manifests six-fold symmetry spots, it is plausible that the protrusions, specifically Fc-amm on Cu(111), exhibit a long-range order in accordance with the substrate's face-centered cubic (fcc) (111) symmetry.

Figure S6, Fc-amm molecules on BrCR/Cu(111).

The deposition quantities of Fc-amm on the 2D-SAM film of BrCR prepared on Cu(111) at 300 K in UHV exhibited a remarkable transition from a 1D chain to a 2D crystal phase. Initially, 0.2 MLs of

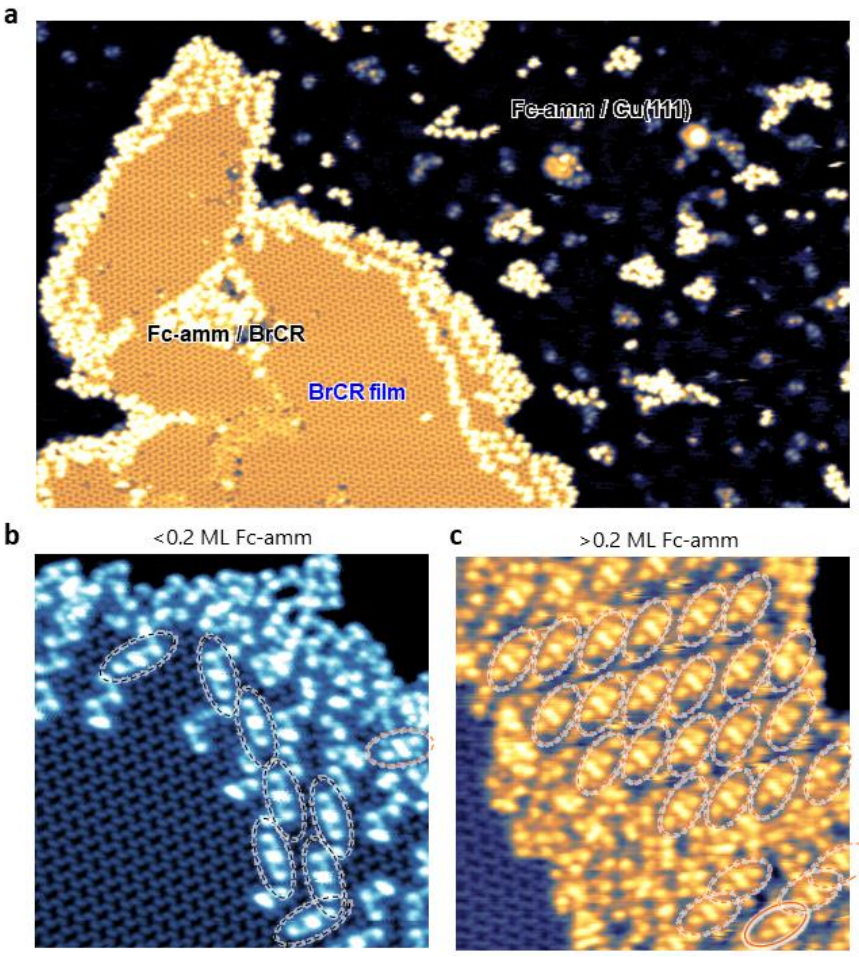

Figure S6. STM topographic images obtained on the Fc-amm molecules deposited on the BrCR array, prepared on the Cu(111) substrate at 300 K in UHV. (a) STM topographic image (60 nm × 40 nm, V_s = 1.8 V, I_t = 12 pA) obtained on the 0.1 MLs Fc-amm / 0.5 MLs BrCR. (b) STM topographic image obtained on the surface the 0.1 MLs Fc-amm / BrCR: 20 nm × 20 nm, V_s = 1.2 V, I_t = 10 pA. (c) STM image obtained on the 0.3 MLs Fc-amm / BrCR: 20 nm × 20 nm, V_s = 1.2 V, I_t = 10 pA.

Fc-amm was deposited on the 2D BrCR array. The STM topographic image in Fig. S6a revealed that the deposited Fc-amm molecules on the BrCR array retained their position on the BrCR island, in stark contrast to the Fc-amm/BrCR arrangement on Au(111) (refer to the main text in Fig. 1). Given the absence of Fc-amm molecules around the central region of the BrCR island, the adsorbed Fc-amm on the BrCR exhibited thermal diffusion. However, upon occupation of the descending step edges of BrCR, interactions between Fc-amm molecules ensued, resulting in their entrapment within the BrCR nanoporous slots. Our observations unveiled that Fc-amm molecules have the capacity to assume diverse assembly structures. Figures S6b and S6c illustrate deposition quantities below and above 0.2 MLs. The former yielded isolated chain structures, while the latter gave rise to a densely packed 2D crystalline array.

Experimentally obtained STM images indicate that the alignment of the Fc-amm array on the BrCR array is approximately $\begin{pmatrix} \boldsymbol{b_1} \\ \boldsymbol{b_2} \end{pmatrix} = \begin{pmatrix} 2.6 & -0.4 \\ 0 & 2.5 \end{pmatrix} \begin{pmatrix} \boldsymbol{a_1} \\ \boldsymbol{a_2} \end{pmatrix}$, showing that the Fc-amm molecules do not strictly adhere to the BrCR sequence. This implies that the dense-packed Fc-amm array may exhibit an inherent regularity similar to the bulk phase, emancipated from the BrCR regularity.

Figure S7, BrCR on Au(111).

STM measurements were conducted on the 2D SAM film of BrCR grown on the Au(111) surface. The monolayer film exhibits a height of approximately 190 picometers with a unit cell of $|a_1|$ = 1.0 nm, $|a_2|$ = 2.2 nm, θ= 88°.

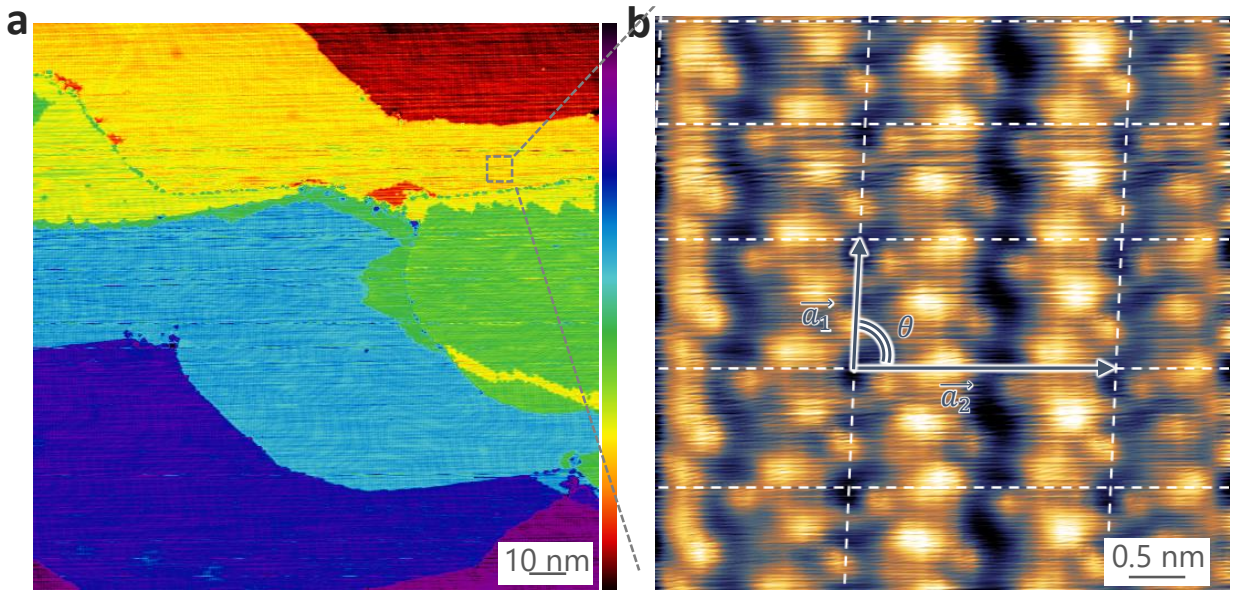

Figure S7. STM topographic images obtained on the Au(111) surface covered by the 0.8 MLs BrCR film. (a) 100 nm × 50 nm, V_s = -2 V, I_t = 10 pA. (b) Enlarged STM image: 5 nm × 5 nm, V_s = -0.8 V, I_t = 100 pA.

Figure S8, Fc-amm molecules on Au(111).

STM was employed to validate the existence of the Fc-amm molecular island formed on Au(111). Figure S8a illustrates two distinct Au(111) terraces, along with the Fc-amm molecular island expanding from the step edge of Au(111). In Fig. S8b, the magnified STM image inside the Fc-amm island revealed numerous protrusions. However, a six-fold symmetry pattern was absent.

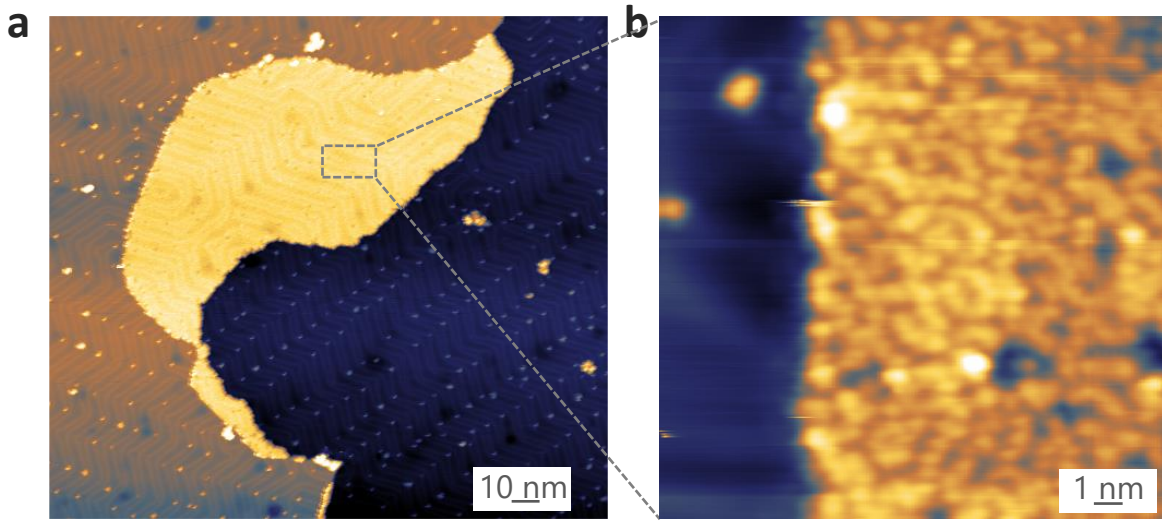

Figure S8. STM topographic images obtained on the Au(111) surface covered by a 0.4 MLs Fc-amm film. (a) 200 nm × 200 nm, V_s = -1.5 V, I_t = 15 pA. (b) Enlarged STM image:10 nm × 10 nm, V_s = -1.0 V, I_t = 70 pA.

Figure S9, Fc-amm adsorption on the BrCR array prepared on Au(111).

Commencing with a gold (Au) substrate surface, a commonplace inert material for junction electrodes, Figure S9 illustrates the deposition of Fc-amm on the BrCR 2D-SAM film on Au(111). While the BrCR forms an ordered array with a unit vector of $\boldsymbol{a_1}$ = 1.01 nm, $\boldsymbol{a_2}$ = 2.23 nm, θ = 88° (Supplementary, Fig. S7), no Fc-amm molecules persist on the BrCR array. All Fc-amm molecules adsorbed on the BrCR array thermally diffuse and traverse descending steps on the Au(111) terraces, eventually forming Fc-amm islands (Fig. S9). These islands exhibit a similar disordered structure to Fc-amm directly deposited on Au(111) (Supplementary, Fig. S8). This experimental evidence suggests that capturing the guest by the host on the 2D surface proves challenging, even if successful in the 3D bulk system, as depicted in Fig. 1b. We posit that the BrCR on Au(111) may assume a structure akin to the

gas phase, namely a bending structure, fostering weak interaction between Au and BrCR, thereby lacking trapping ability.

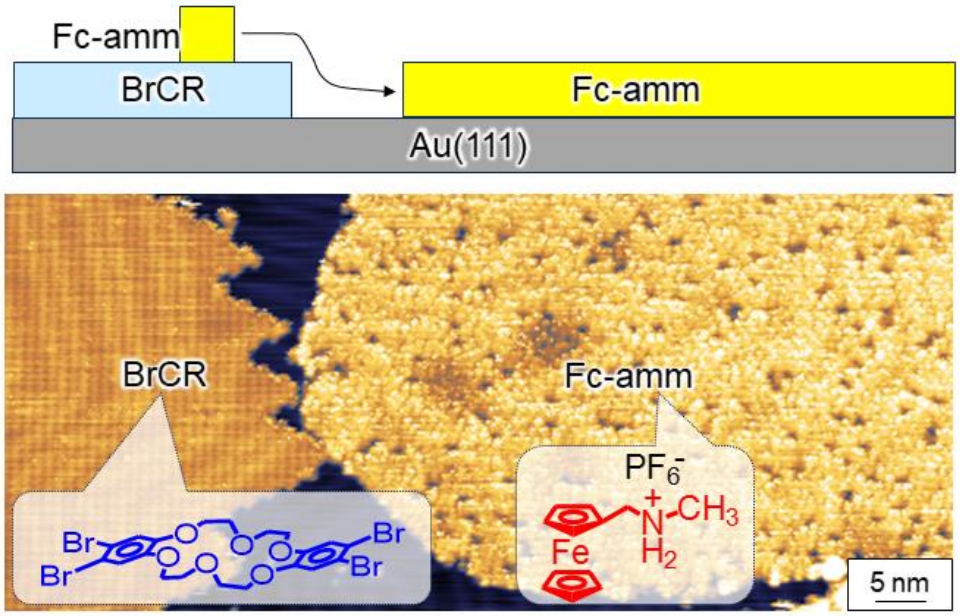

Figure S9. STM topographic image and the correspondent cross-section view model: 0.8 MLs BrCR film on Au(111) after depositing the 0.3 MLs Fc-amm (80 nm × 40 nm, Vs = -2.0 V, It = 12 pA).

Figure S10, Calculated DOS of the bulk Fc-amm crystal.

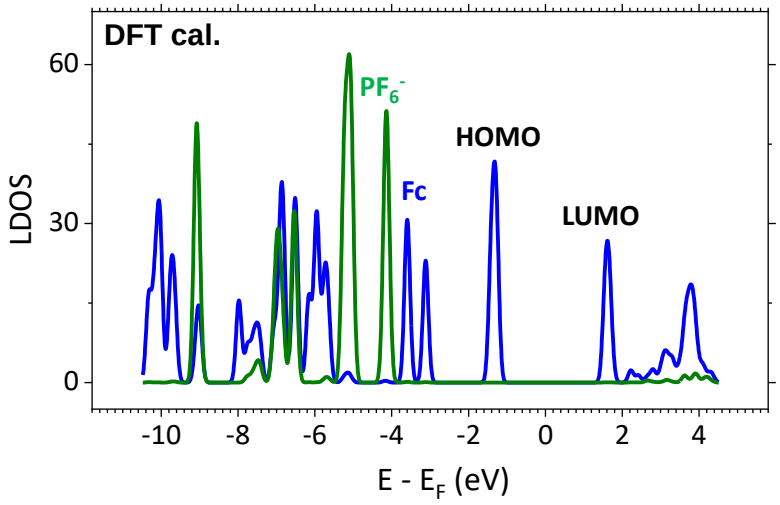

Figure S10. DFT calculation results of Fc-amm bulk crystal. Blue and green lines denote LDOS at ferrocene and PF_6^- ligand positions, respectively.

Supplementary Note: XPS results of Fc-amm on BrCR/Cu(111).

To confirm the composition of the Fc-amm molecules on the sample, the XPS spectra for F 1*s* and Fe 2*p* of (a) the Fc-amm/Au(111), (b) Fc-amm/Cu(111), and (c) Fc-amm/BrCR/Cu(111) are compared in Fig. S11.

In contrast to STM, XPS provides integrated results from the entire sample. Also, light irradiation causes molecular decomposition during the measurement. From these two points, it can be challenging to correspond quantitatively to the results obtained by STM. However, the XPS results imply that we observed in STM that Fc on BrCR is not decomposed.

First, Fc-amm adsorbed on the Au surface could take weak physisorption, resembling the bulk crystal. Indeed, energy positions of (i) Fe 2*p* (red curves) and (iii) F 1*s* peaks (green curve) observed in Fig. S11a correspond to the peak positions of the Fc derivatives (ca. 707 eV and 720 eV) [2] and PF_6 (ca. 687 eV) [3] materials. The fitting with the Doniach-Sanjic function reveals the area ratio between $2p_{3/2}$ and $2p_{1/2}$ doublet of 2:1.

On the contrary, Additional peaks of (ii) Fe 2*p* (blue curve) resolved by the Doniach-Sanjic function fitting, and the (iv) F 1*s* peak (green curve) appeared on the Cu and BrCR/Cu surfaces as depicted in Figs. S11b and S11c.

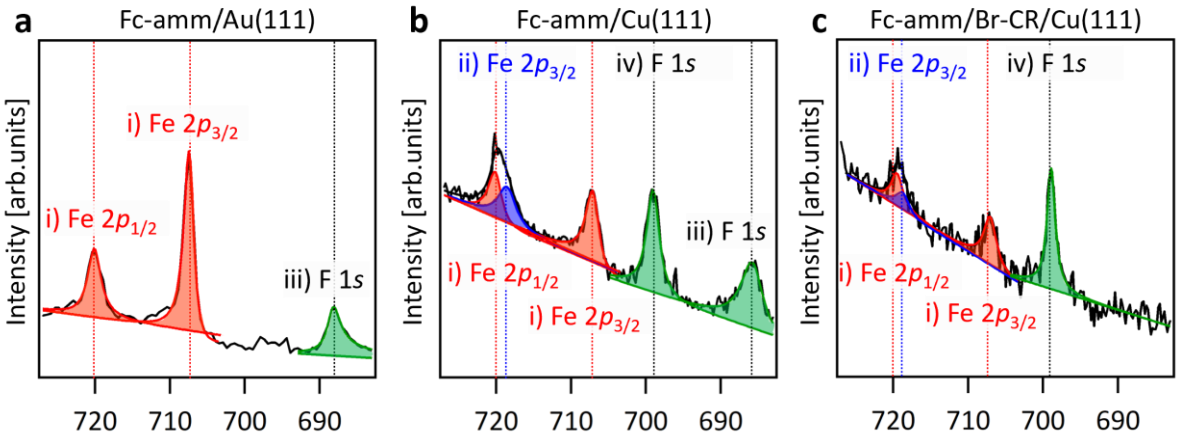

Figure S11. XPS core level spectra for F 1*s* and Fe 2*p* region measured at room temperature with an excitation energy of 1253.6 eV. (a-c) XPS spectra acquired on the (a) 4 MLs Fc-amm / Au(111), (b) 0.3 MLs Fc-amm / Cu(111), (c) 0.3 MLs Fc-amm / 1 ML BrCR / Cu(111). The Fe 2*p* peaks are fitted by the spin-orbit doublets (black solid line shows the total fitted curve, while red and blue solid lines are the fitted curve for each peak).

Table S2. The number of F atoms per an Fe atom within the Fc-amm evaluated from the area ratio between the experimentally obtained Fe 2*p* and F 1*s* peaks in Fig. S11.

Sample	F/Fe ratio
Fc-amm/BrCR/Cu(111)	3.1
Fc-amm/Cu(111)	3.2
Fc-amm/Au(111)	1.2

We could estimate how many F atoms are included inside Fc-amm from these areas of the peaks. If all Fc-amm on the surface consists of PF_6, the ratio of F/Fe should be six.

For example, in Fig. S11b, the ratio between the Fe 2*p* peak areas and the F 1*s* peak area is 1:0.87. Then, we take into account the different cross-sections for the F: 0.095 and Fe: 0.35 for the 1253.6 eV X-ray, which gives rise to the ratio of F/Fe ~ 3.2 (Table S2).

We look at the first case of Fc-amm/Au(111), which shows the F/Fe ratio of 1.2, much lower than the ideal ratio of six. This could indicate the partial decomposition of the PF_6 ligand during the thermal sublimation at 348 K in UHV and the X-ray irradiation during the XPS measurements (about three h). Hence, only 1/6 ~ 17% of Fc-amm with PF_6 might remain on the surface. This lower F/Fe ratio suggests that F 1*s* peak (iii) in Fig. S11a could be attributed to not only the PF_6 but also to PF_2 and/or PF_4 in the F-depleted state due to photoirradiation and sublimation, where the binding energy would be similar to each other and located at the lower energy side of the peak tail. It should be noted that the XPS results of Fc-amm/Au(111) indicate that there is no damage from the Au substrate to the Fc-amm, while the X-ray or heating could decompose the PF_6 ligand.

Also, we take the F/Fe ratio from the Fe 2*p* peaks (i) and (ii), and F 1*s* (iv) on the Fc-amm/Cu(111) (Fig. S12b) and Fc-amm/BrCR/Cu(111) (Fig. S12c). The former and latter show a ratio of 3.2 and 3.1, three times larger than the 1.2 obtained on the Fc-amm/Au(111), indicating the isolated F atoms could remain on the surface due to the more robust interaction with the Cu.

No literature and XPS database are reported for a newly formed F 1*s* peak iv). A possible explanation would be that F 1*s* are strongly chemically bonded to ammonium and the ether groups in the crown molecule due to a surface coordination reaction. Only the sharp oxidation-derived peak iv) is identified on the BrCR film, so the F-derived spots estimated as PF_6 in Fig. 3 in the main manuscript might

consist of oxidized fluorenes. As a reference, to the best of our knowledge, a functional group of the PF_2N cluster only reported the F 1*s* binding energy to be 695 eV [1].

We also compared the two Fe 2*p* peaks of the ordinary (i, red curves) and the extra (ii, blue curve). The area ratio of Fe $2p_{3/2}$ peak (i) to Fe $2p_{3/2}$ peak (ii) decreases 1/3 (=0.2/0.6) on the Fc-amm/BrCR/Cu(111) compared to the Fc-amm/Cu(111). Namely, the strong oxidization could be due to the Cu substrate. Moreover, this ratio increased with increasing the X-ray irradiation time of the measured sample, and we did not observe this extra Fe peak (ii) on the Au surface; the appearance of the additional Fe peak, indicating a strong oxidization of iron, could be due to the Cu substrate [4,5], and which is not directly related to the Fc-amm on BrCR, as studied using STM in this manuscript.

No chemical bonding between Fc-amm and BrCR

To assess the chemical state of the BrCR films before and after Fc-amm adsorption, XPS measurements of the O 1*s*, Br 3*p*, and C 1*s* peaks are carried out for the one monolayer BrCR on Cu(111) (blue line) and 0.3 MLs Fc-amm on 1 ML BrCR/Cu(111) (green line) as depicted in Fig. S12. For O 1*s* and Br 3*p* contained in the BrCR molecule, no apparent change in the spectral shape and peak position before and after Fc-amm adsorption is detected. Also, the C 1*s* peak (i) described from the BrCR molecule shows no evident change after deposition of the Fc-amm molecule. On the other hand, the intensity of peak (ii) slightly increased after Fc-amm adsorption, as the C 1*s* peak derived from Fc-amm molecules appeared at around the peak (ii), indicating no clear evidence to form any C-F

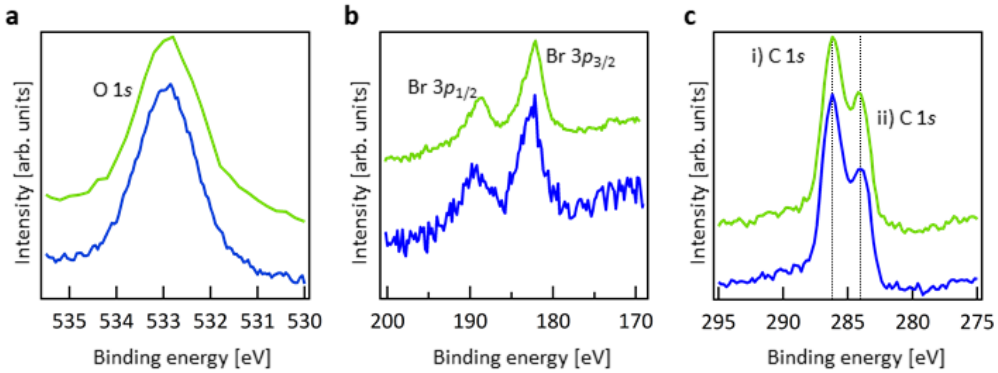

Figure S12. XPS core level spectra for (a) O 1*s* and (b) Br 3*p* (c) C 1*s* acquired on 1 ML BrCR/Cu(111) (blue line) and 0.3 MLs Fc-amm / 1 ML BrCR / Cu(111) (green line), respectively, measured at room temperature with an excitation energy of 1436.6 eV.

compounds by decomposition of PF_6 [1]. All the results show no chemical bond between the BrCR and Fc-amm molecules, demonstrating that Fc-amm is physisorbed on the BrCR film.

References:

[1]: D. T. Clark *et al*., J. Electron Spectrosc. **1,** 227 (1972).

[2]: C. M. Woodbridge *et al*., J. Phys. Chem. B **104**, 3085 (2000).

[3]: B. S. J. Heller *et al*., Chem.Eur.J. **26**,1117 (2020).

[4]: D. Welipitiya *et al*., J. Appl. Phys. **79**, 11 (1996).

[5]: K.-F. Braun *et al*., Phys. Rev. Lett. **96**, 246102 (2006).

Figure S13, Fc-amm/BrCR complex in bulk single-crystal based on X-ray diffraction results.

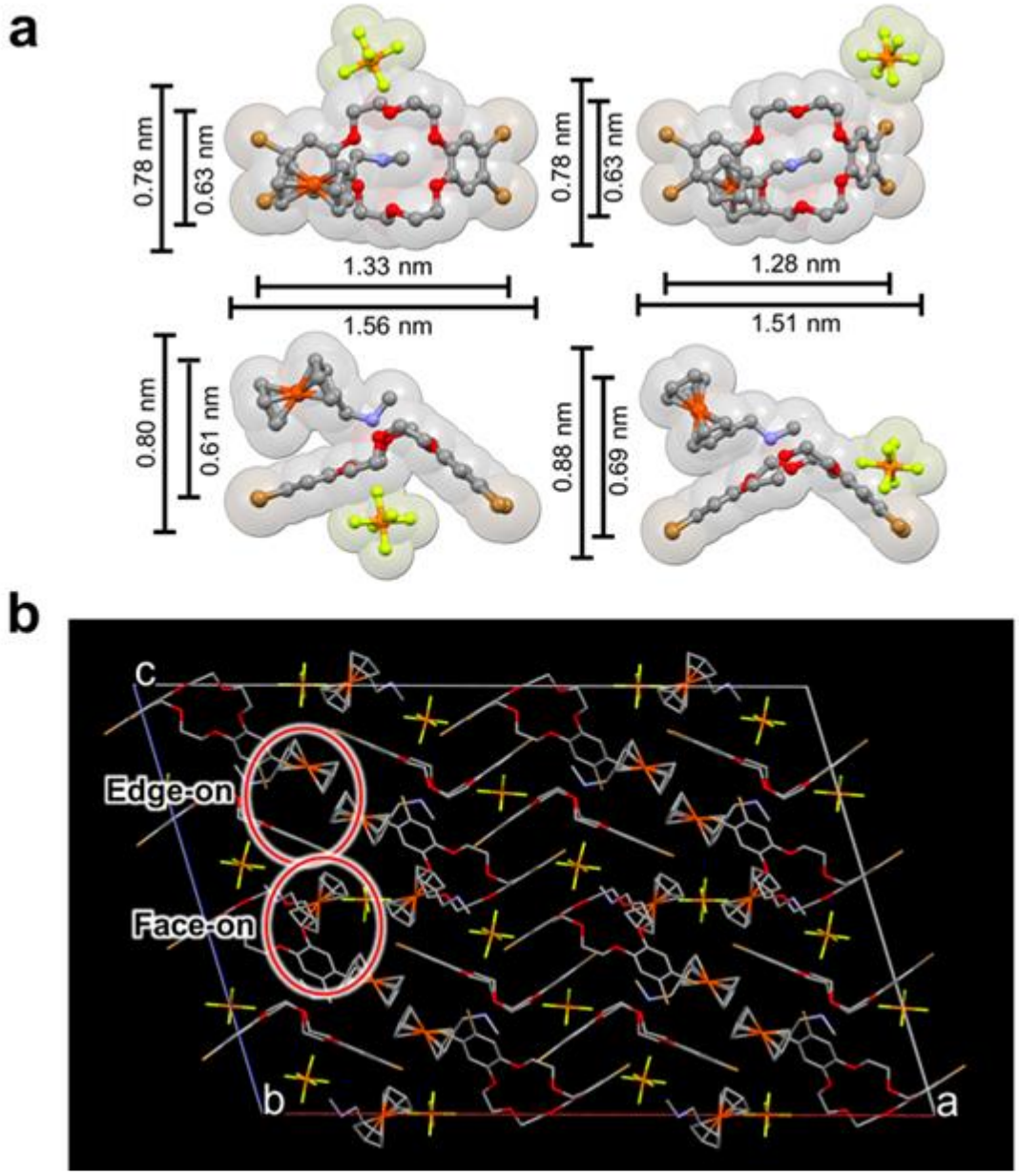

Figure S13. Single-crystal X-ray crystallographic structures of (a) Fc-amm/BrCR complexes and (b) their packing structure in a unit cell.

Figure S14, DFT results of Fc-amm single molecule on BrCR / Cu(111).

In the DFT calculations of Fc-amm/BrCR/Cu(111), we obtained eight solutions for the structural optimization, starting from various initial conditions. The eight structures are shown in Fig. S14. The two most stable ones, No.1 and No.2, are discussed in the main text. The other six structures are considerably less stable. In structure No.7, the Fc is above the benzene ring (as in 1,2), but the amm-

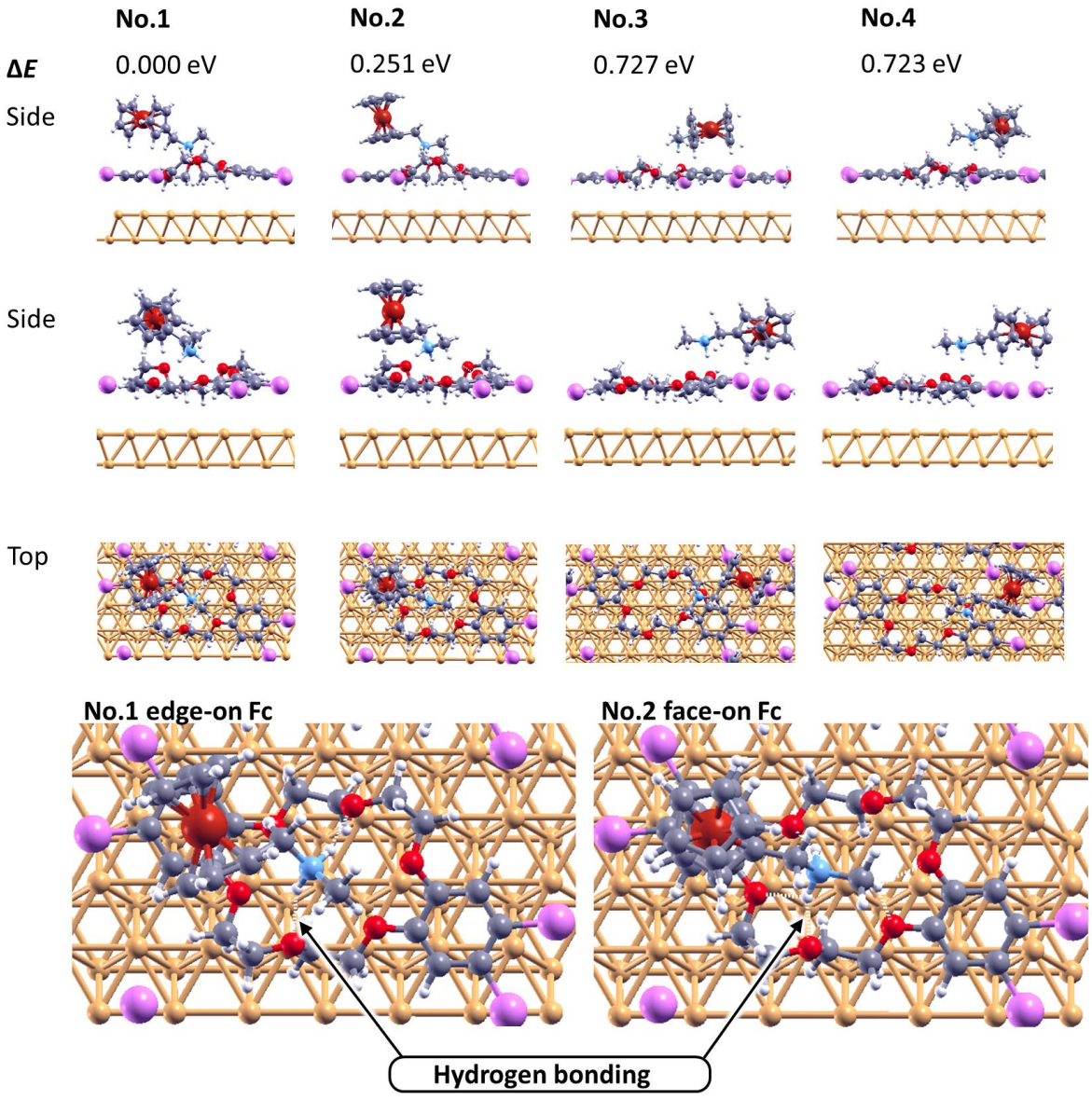

Figure S14. DFT results of eight configurations (No.1-4) of Fc-amm single molecule on BrCR / Cu(111). Δ*E* denotes the energy difference from the most stable configuration (No.1). Upper panels show side and top views of each configuration. Lower panels show magnified views of the most energetically stable edge-on (No.1) and the second stable face-on (No.2) configuration, in which a white line denotes the hydrogen bonding.

group is outside the crown ring, above the Br atoms. This is less stable than structure No.1 by 1.02 eV. If the Fc is not located above the benzene ring but above or between the Br atoms (structures No.3 and No.4), then the energy is 0.72-0.73 eV higher. Suppose the amm-group is turned 90 degrees or more relative to the stable, regular Fc-amm conformation. In that case, the energy also goes up by at least 0.849 eV (structures No.5 and No.6). If the Fc molecule is shifted away from the center of the benzene ring by 0.2 nm. The system is much less stable by 1.642 eV (structure No.8). From the relative energies (ΔE) of the various structures, we may infer that the most robust interaction is the π-π bonding between the benzene ring and Fc, followed by the hydrogen bonds of the amm-group with the crown ring. We conclude that the stable adsorption site of Fc-amm on BrCR/Cu is the edge-on orientation with the Fc molecule over the benzene ring and the amm-group over the crown, corresponding to a host-guest interaction.

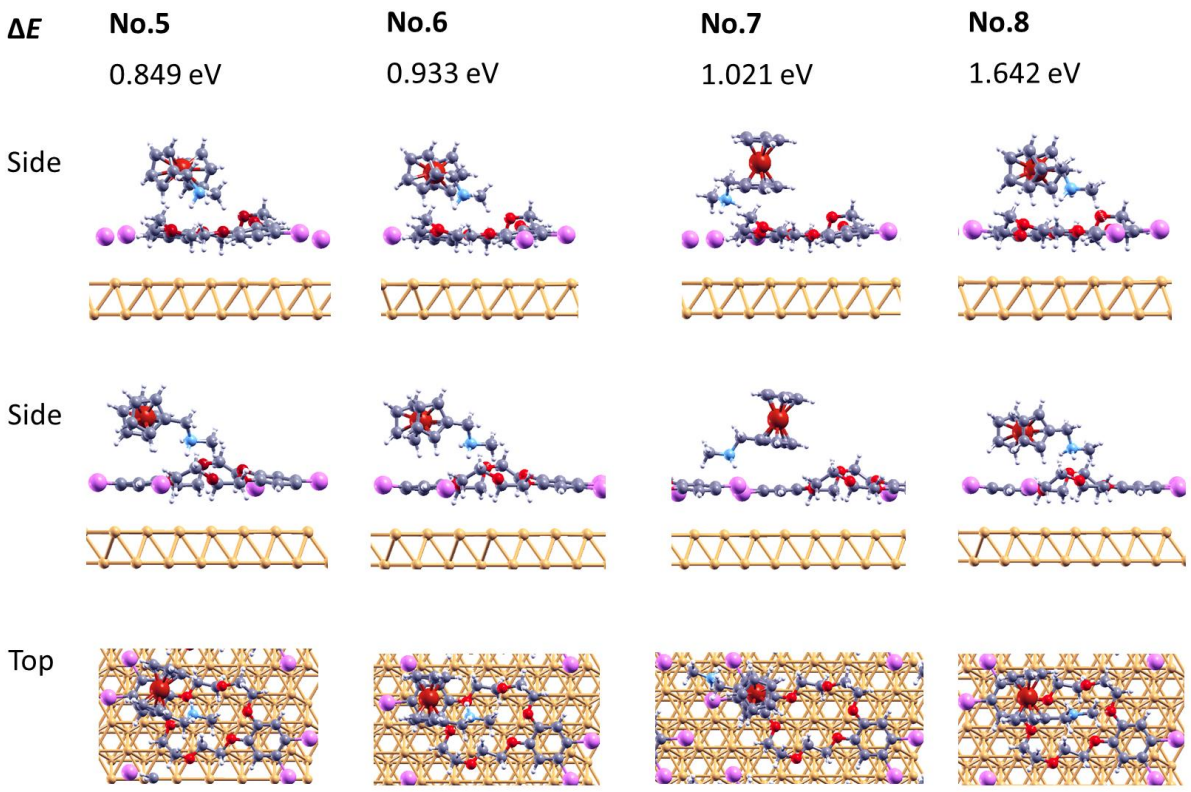

Figure S15. DFT results of eight configurations (No.5-8) of Fc-amm single molecule on BrCR / Cu(111). ΔE denotes the energy difference from the most stable configuration (No.1). Upper panels show side and top views of each configuration.

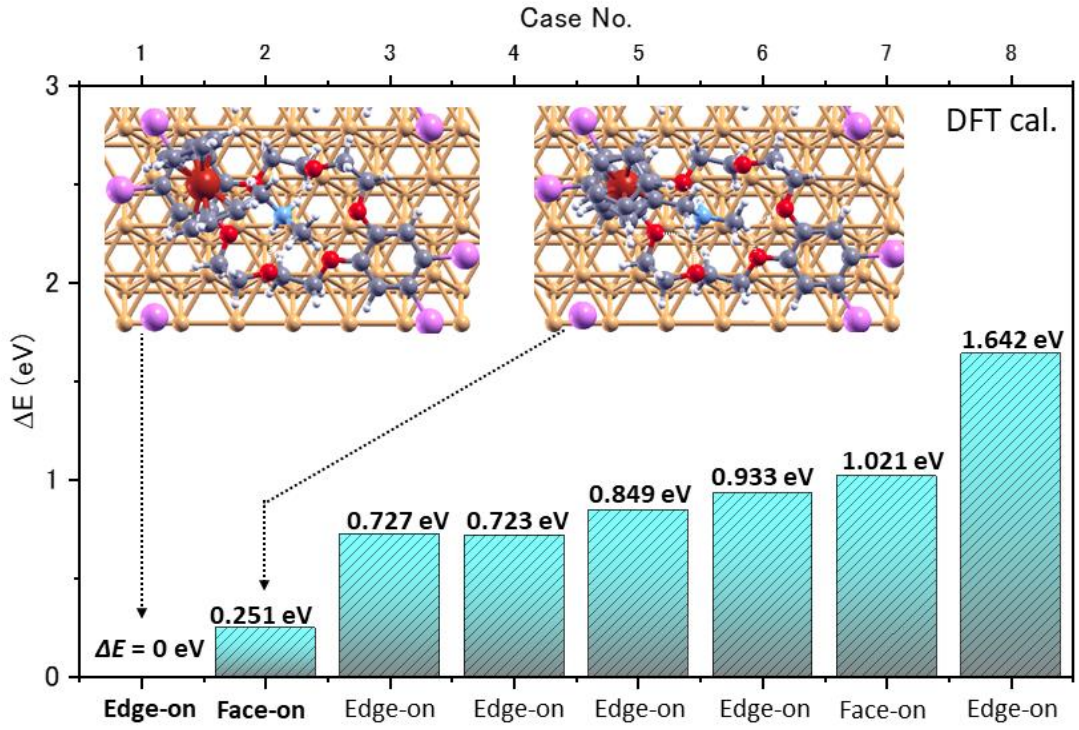

Figure S16. Histogram of the energy difference between eight configurations (No.1-8) in Figs. S14-S15. Δ*E* denotes the energy difference from the most stable configuration (No.1).